Effect of the Growth Temperature on the Diameter Distribution and Chirality of Single-Wall Carbon Nanotubes

Shunji Bandow[1,*] and S. Asaka[2]
[1]*Research Center for Molecular Materials, Institute for Molecular Science, Myodaiji, Okazaki 444, Japan*
[2]*Equipment Development Center, Institute for Molecular Science, Myodaiji, Okazaki 444, Japan*

Y. Saito
Department of Electrical and Electric Engineering, Mi'e University, Tsu, Mi'e 514, Japan

A. M. Rao,[3,4] L. Grigorian,[3] E. Richter,[3] and P. C. Eklund[3,4,*]
[3]*Department of Physics and Astronomy, University of Kentucky, Lexington, Kentucky 40506-0055*
[4]*Center for Applied Energy Research, University of Kentucky, Lexington, Kentucky 40506-0055*
(Received 18 November 1997)

Pulsed laser vaporization of a heated, Fe/Ni or Co/Ni catalyzed, carbon target in argon gas has been used to synthesize single-wall carbon nanotubes (SWNTs). Electron microscopy, x-ray diffraction, and Raman spectroscopy were all used to study the effect of the catalyst on the tube yield, and the evolution of the tube diameter distribution with increasing growth environment temperature T. By controlling the temperature in the range $780 < T < 1050\,^{\circ}\mathrm{C}$, we have been able to tune the diameter of the tubules from ~ 0.81 to ~ 1.51 nm. The threshold temperature for significant SWNT production was found to be $\sim 850\,^{\circ}\mathrm{C}$. [S0031-9007(98)05909-2]

PACS numbers: 61.48.+c, 81.05.Tp

In 1996, Smalley and collaborators reported that the pulsed laser vaporization (PLV) of a heated ($\sim 1200\,^{\circ}\mathrm{C}$) carbon target containing a few percent Ni-Co catalyst could be used to produce single-wall carbon nanotubes (SWNTs) that are organized into a regular triangular lattice to form "ropes" or "bundles" [1]. The diameter distribution of these tubes was reported to be peaked sharply at ~ 1.36 nm, close to the diameter predicted for a (10,10) "armchair" tube [2]. Theoretical arguments were presented which showed that the (10,10) tube was thermodynamically favored, and the growing edge of the tubules was stabilized by C≡C triple bonds [1]. Raman scattering studies [3] on these bundles of tubules showed clearly that a *distribution* of tube diameters near that of a (10,10) tubule was required to explain the Raman spectra, and this view was confirmed in that work by transmission electron microscopy (TEM).

In this paper, we report on the influence of the laser target and tube growth environment temperature (T) on the diameter and symmetry of SWNTs produced by the PLV method. A two pulse sequence from a Nd:YAG laser (532 nm radiation followed by 1064 nm radiation at 20 Hz and coaxial with the 532 nm radiation) was focused in a 3 mm diameter spot on carbon targets containing either Fe/Ni (0.6/0.6 at. %) or Co/Ni (2.6/2.6 at. %). Each target was placed in a quartz tube near the center of a 30 cm tube furnace. Flowing Ar gas [100 SCCM, 500 Torr (SCCM denotes cubic centimeter per minute at STP)] was introduced at the front of the furnace that carried the SWNTs and other carbon products produced in the carbon plasma to the rear of the furnace, where they were collected just outside on a water-cooled Cu cold finger. The average temperature near the carbon target and growth environment T was controlled to within $\pm 1\,^{\circ}\mathrm{C}$, and was measured by an optical pyrometer which was calibrated against a thermocouple.

For temperatures $T \leq 850\,^{\circ}\mathrm{C}$, the deposit appeared more similar to a carbon soot in the scanning electron microscope (SEM) images (Hitachi Model S-900 at 5 kV). According to SEM images, the fractional carbon yield in tubules, relative to that in carbon nanospheres, was drastically accelerated for $T > 850\,^{\circ}\mathrm{C}$ (Fig. 1, solid circles, left-hand scale). The number of tubes in a bundle was also observed to increase above $780\,^{\circ}\mathrm{C}$ (Fig. 1, open

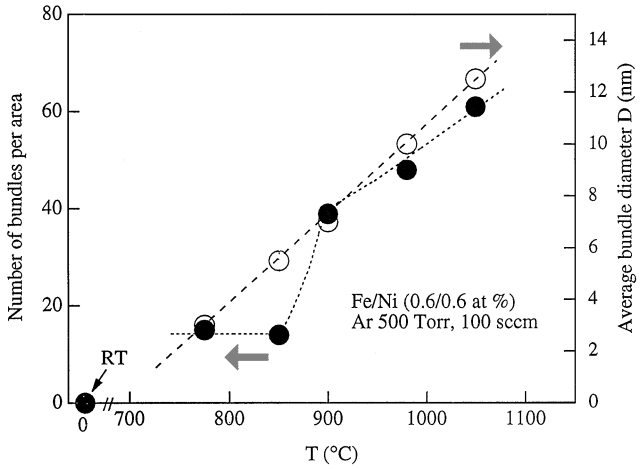

FIG. 1. Fractional nanotube yield (solid circles, left-hand scale) and average bundle or rope diameter D vs target/growth environment temperature T (open circles, right-hand scale) for Fe/Ni catalyzed carbon target.

circles, right-hand scale). Using the right-hand vertical scale in Fig. 1, we plot the average bundle or rope diameter D vs T, where the number of tubes per bundle is approximately proportional to D^2. Furthermore, at temperatures as low as $T = 780\,^{\circ}\mathrm{C}$, 3 to 5% of SWNT yield was still observed. When the average target temperature was near room temperature, an extensive search failed to uncover any SWNTs in the carbon soot.

In Fig. 2, we present the tube diameter distribution inferred from fringe spacing in the TEM lattice images (Phillips EM400 microscope at 120 kV) on bundles of tubes prepared from Fe/Ni catalyzed carbon targets for various T. Results for Ni/Co targets were found to be very similar and, for brevity, are not shown here. The histogram plots in Fig. 2 represent the diameter distribution obtained from direct lattice images of nanotube bundles lying parallel to the focal plane of the microscope. In Fig. 2, the bottom three insets show the (11) x-ray diffraction (XRD) peak associated with the intertubule spacing (d_{11}; top inset in Fig. 2) within a bundle. The position of the (11) XRD peak was used to estimate the "average" SWNT diameter produced in the macroscopic sample at each target temperature, and this value is represented by a dashed vertical line in the figure [4]. For the lowest growth environment temperature $T = 780\,^{\circ}\mathrm{C}$, the (11) diffraction peak could not be detected above the background. This observation is consistent with the TEM observations that the tube bundles synthesized from the lowest temperature target contained relatively much fewer tubes. The increase of the average tube diameter with increasing T is also evident from the TEM histogram data in

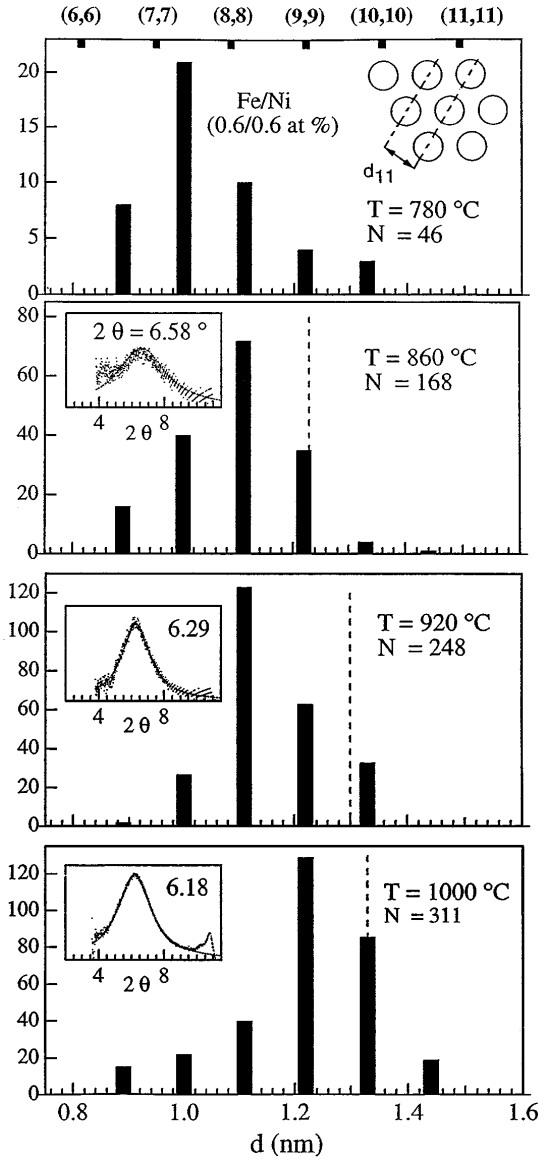

FIG. 2. Diameter distribution for nanotubes produced using Fe/Ni catalyst for several target/growth environment temperatures T. The left insets show the (11) x-ray diffraction peak for these samples and the dashed vertical line represents the average diameter for the nanotubes calculated from the position of the (11) peak [4]. In the right inset, d_{11} is the distance between the [11] planes of tubes in the bundle. In each panel, N represents the number of tubes measured.

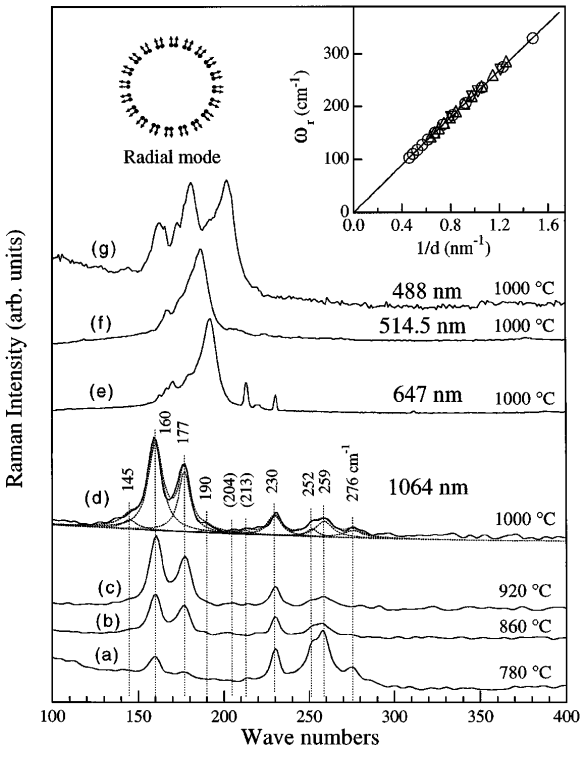

FIG. 3. Low frequency, room temperature Raman spectra for nanotubes produced using Fe/Ni catalyst at the temperatures indicated. The spectra are unpolarized and were collected in the backscattering configuration. Spectra (a)–(d) were taken using the 1064 nm excitation on samples prepared at $T = 780$, 860, 920, and 1000 °C, respectively. Spectra (e)–(g) are for the same sample produced at $T = 1000\,^{\circ}\mathrm{C}$ but using 647, 514.5, and 488 nm excitations, respectively. The right inset shows the calculated radial frequency vs tube diameter for armchair (○), zigzag (△), and chiral (▽) symmetry tubes.

the figure. The most frequent tube diameter can be seen to shift from that of a $\sim(7,7)$ tube to that of a $\sim(9,9)$ tube as T increases from 780–1000 °C. Furthermore, the width of the diameter distributions was found to not be particularly sensitive to T. As can be seen in Fig. 2, a clear offset between the most frequent tube diameter (from TEM) and $\langle d_t \rangle$ (from XRD) is detected. The reason for this offset is not yet fully understood. Computer simulations of the TEM lattice fringe images at various focal conditions will be necessary to resolve the apparent offset. However, both the x-ray and the TEM data show clearly that an increase in the mean tube diameter with increasing target and growth temperature has occurred. Even using the larger $\langle d_t \rangle$ values obtained from XRD, none of the samples synthesized in this work were found to yield an *average* tube diameter as large as a (10,10) tube. However, it should be noted that the temperature of the carbon target and growth environment favorable for the growth of a (10,10) tube has been reported to be 1200 °C [1], some 200 °C hotter than our highest T data. Given the trends in our data, a 1200 °C environment might be expected to produce a mean diameter close to that of a (10,10) tube.

Raman scattering from vibrational modes of small diameter SWNTs have been reported recently and have provided important information about the diameter dependence of the vibrational mode frequencies and excited electronic states of these carbon tubes [3,5], and also the effect of chemical doping [6]. The Raman scattering has been shown experimentally to be a resonant process and this has been associated with optical transitions between one-dimensional (1D) states in the electronic band maxima and minima [3]. In the present Letter, we have extended our force constant model calculations for the radial breathing mode frequency (ω_r) to the other two general subclasses of tubes: "zigzag" $(n,0)$ and "chiral" (n,m). In the right inset in Fig. 3, we plot the calculated radial breathing mode frequency (ω_r) vs the inverse tube diameter $(1/d)$ for all symmetry types; i.e., (n,n), $(n,0)$, and (n,m). As can be seen from the right inset in Fig. 3, the calculated frequencies all fall on a straight "universal" line well fit by the function $\omega_r = 223.75(\mathrm{cm}^{-1}\,\mathrm{nm})/d(\mathrm{nm})$. As anticipated, for $d = \infty$, $\omega_r = 0$, as this frequency corresponds to the $q = 0$ transverse acoustic phonon of a flat graphene sheet and this mode thereby corresponds to a rigid displacement of the sheet normal to its surface. Our calculations show clearly that ω_r is only sensitive to inverse diameter and is *not* sensitive to the helicity (or symmetry) of the particular tube. Thus, this Raman-active radial mode, which can exhibit quite a large resonant Raman cross section [3,5], is ideal for determining the diameter of SWNTs.

In Fig. 3, we display the low frequency region of the Raman spectrum for SWNTs, where the resonantly enhanced lines associated with the radial breathing modes of various diameter SWNTs are expected. These spectra were chosen to show the strong resonance effects (i.e., peak shifting and intensity change) as discussed in Ref. [3]. As the data in Fig. 3 indicate, to find all of the radial mode frequencies associated with a given sample, it is necessary to use several excitation wavelengths. The peak positions were obtained from a Lorentzian line shape analysis [for

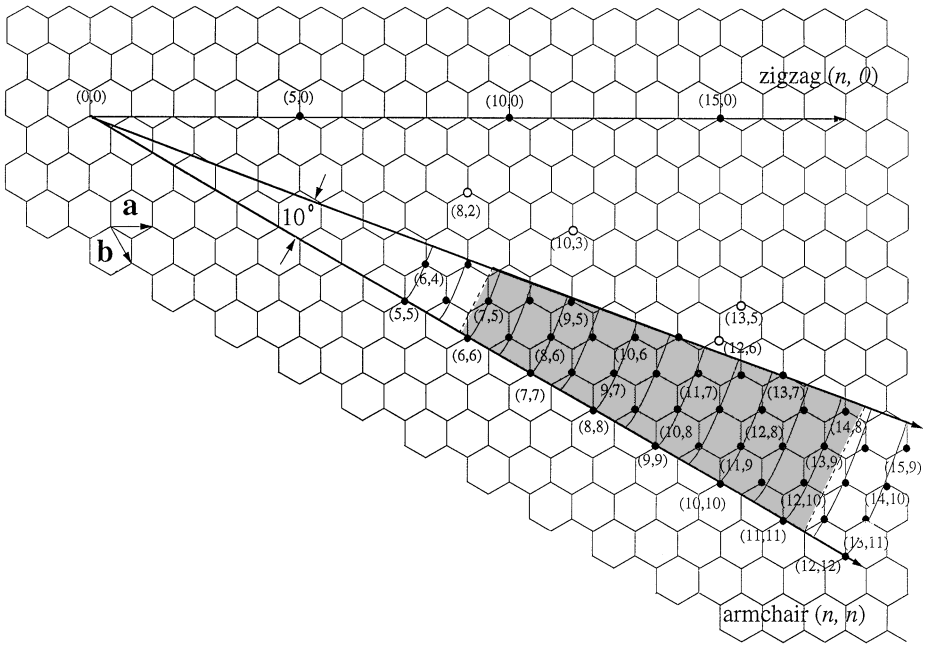

FIG. 4. Chiral vector map for carbon nanotubes with diameter $d < 1.65$ nm. The arcs locate tubes of the same diameter d and theory predicts $\omega_r \sim 1/d$. The experimentally observed frequencies in Fig. 3 are attributed to the 11 resolvable breathing mode frequencies ω_r for tubes occupying the shaded 10° wedge closest to the armchair (n,n) direction.

example, Fig. 3(d)] for tubes produced both for the Fe/Ni and the Co/Ni catalyzed targets. They have all been identified with the resonantly enhanced radial breathing mode for tubes with differing diameter [7]. Other lower symmetry, low frequency modes exhibit a significantly weaker Raman scattering cross section [3]. From the calculated relation $\omega_r \sim 1/d$, it is evident that smaller (larger) diameter tubes should exhibit higher (lower) radial mode frequencies, which might be appreciated intuitively. Thus the evolution of the spectra in Figs. 3(a)–3(d), i.e., the shift of intensity towards lower frequency radial modes with increasing T, signals the increased production of larger diameter tubes, consistent with the XRD and TEM data in Fig. 2.

In Fig. 4, we display a map of chiral vectors **C** which can be used to identify all possible SWNTs with diameter $d \leq 1.65$ nm using the standard carbon nanotube notation involving the pair of integers (n, m) [2]. The unit cell, tube axis, and diameter of an (n, m) tube are all uniquely specified by **C** [8]. The solid dots (•) locate the tips of $\mathbf{C}(n, m)$ for all zigzag $(n, 0)$, armchair (n, n) and chiral $(n, m \neq n)$ tubes with $d < 1.65$ nm. As discussed below, most of the vectors relevant to this work can be assigned to the ~10° wedge closest to the so-called *armchair* tube direction (n, n). This 10° wedge angle is consistent with the range of helix or chiral angles reported by Cowley *et al.* [9] for SWNTs prepared by PLV at $T = 1200$ °C. The tube diameter d is related to the length of the chiral vector **C** by the simple relationship $d = |\mathbf{C}|/2\pi$ [2]. Thus, the thin circular arcs in Fig. 4 represent constant tube diameters. Since $\omega_r \sim 1/d$, these arcs also represent constant radial frequency arcs. It is interesting to see that, within this 10° wedge, the tubes are organized very nearly on "constant frequency" arcs. Thus, we expect all tubes within this wedge with diameters between that of a (5,5) and a (12,12) tube to exhibit only 15 different radial mode frequencies. Furthermore, since the electron-phonon broadening in graphite is ~6 cm^{-1} [10], we do not anticipate resolving the four frequencies, for example, on the (10,10) arc inside the 10° wedge. It should be noted that 7 of the 15 anticipated frequencies stem from arcs which do not contain an armchair tube; i.e., they must be chiral symmetry tubes. A few experimental frequencies we observe cannot be explained by tubes which fall within this 10° wedge closest to the armchair direction. They are highlighted in the chiral map (as open circles in Fig. 4).

Taken collectively, the data presented in this Letter show that the mean diameter of nanotubes increases with increasing temperature of the growth environment in the PLV process, and the tubes collect into bundles at all growth temperatures used in this study. A broad range of carbon nanotube diameters with uniform diameter distribution have been observed and the Raman data are interpreted to indicate that they fall primarily in a wedge of the chiral vector map within 10° of the armchair direction.

The work at IMS was supported by the Grant-in-Aid for Scientific Research (C) Grant No. 08640749 from the Japanese Ministry of Education, Science, Sports, and Culture. The Kentucky group was supported by the University of Kentucky Center for Applied Energy Research and NSF Grant No. OSR-94-52895.

*To whom correspondence should be addressed.

[1] A Thess *et al.,* Science **273**, 483 (1996).

[2] The notation (n, m) defines the atomic coordinates for the 1D unit cell of the nanotube. For $n \neq m \neq 0$, the tube has chiral symmetry. Achiral tubes exist if $m = 0$ (zigzag) or $n = m$ (armchair). See, for example, M. S. Dresselhaus, G. Dresselhaus, and P. C. Eklund, *Science of Fullerenes and Carbon Nanotubes* (Academic, New York, 1996), Chap. 19.

[3] A. M. Rao *et al.,* Science **275**, 187 (1997).

[4] The (11) diffraction peaks (insets in Fig. 2) were obtained from randomly oriented bundles using Cu x-ray source. After subtraction of a broad background, the (11) peak profiles were found to be well fit by a Lorentzian line shape. The average tube diameter $\langle d_t \rangle$ was calculated from the (11) peak position according to the relation $\langle d_t \rangle = d_{11}/\cos 30° - s$, where s is the intertubule (van der Waals) spacing taken to be 0.32 nm and d_{11} is the distance between [11] planes of tubes in the bundle. The value of $s = 0.32$ nm used is midway between the interplanar spacing in graphite (0.335 nm) and the interfullerene distance in solid C_{60} (0.29 nm).

[5] E. Richter and K. R. Subbaswamy, Phys. Rev. Lett. **79**, 2738 (1997).

[6] A. M. Rao *et al.,* Nature (London) **388**, 257 (1997).

[7] A. M. Rao *et al.,* Thin Solid Films (to be published).

[8] The chiral vector $\mathbf{C}(n, m) = n\mathbf{a} + m\mathbf{b}$, where vectors **a** and **b** are the primitive lattice vectors of a graphene sheet. The chiral angle θ is measured with respect to the zigzag axis (see Fig. 4).

[9] J. M. Cowley, P. Nikolaev, A. Thess, and R. E. Smalley, Chem. Phys. Lett. **265**, 379 (1997).

[10] M. S. Dresselhaus and G. Dresselhaus, Adv. Phys. **30**, 139–326 (1981).